Pol. J. Environ. Stud. Polit. Econ. Ind. Vol. XX, No. X (XXXX), 1-15
DOI: *10.15244/peai/218181* ONLINE PUBLICATION DATE: 2026-04-02

Original Research

Spatiotemporal Characteristics and Driving Factors of Provincial-Level Carbon Dioxide Emissions in China Based on Multi-Source Remote Sensing Data

Jing Zhu[1, 2]*, Jie Luo[3], Xinning Zhao[1], Jia Wang[4], Nianlong Han[5]

[1]School of Business Administration, Northeastern University, Shenyang, 110819, China
[2]School of Economics, Northeastern University at Qinhuangdao, Qinhuangdao, 066004, China
[3]School of Humanities and Law, Northeastern University, Shenyang, 110819, China
[4]School of Management, Shenyang University of Technology, Shenyang, 110870, China
[5]School of Geography and Tourism, Huizhou University, Huizhou, 516007, China

Received: 04 January 2026
Accepted: 16 February 2026

Abstract

Provincial-level carbon reduction policies in China are pivotal to achieving the national goals of carbon peaking and carbon neutrality. Understanding the spatiotemporal characteristics and influencing factors of provincial carbon emissions is essential for formulating and implementing effective emission reduction strategies. This study employs multi-source remote sensing data and selects Liaoning Province, a region with representative carbon emissions, as the research area. Grid-scale emission characteristics are analyzed using the center-of-gravity shift model, standard deviation ellipse model, hotspot/coldspot analysis, and global spatial autocorrelation. The Multi-Scale Geographically Weighted Regression model is applied to examine the influencing factors. The results show: (1) carbon emissions increased continuously during the study period, although the growth rate declined significantly after 2010. The spatial distribution displayed a migration trend from the northeast toward the southwest. (2) The effects of various influencing factors on carbon emissions varied. Electricity consumption exhibited a strong positive correlation. The energy consumption structure showed a positive correlation in most years. Annual Gross Primary Productivity showed a significant negative correlation, and urbanization rate presented both positive and negative effects across different regions. These findings deepen the understanding of the spatiotemporal distribution characteristics and driving mechanisms and provide a valuable reference for developing emission reduction policies in high-emission regions of China.

Keywords: carbon dioxide emissions, spatiotemporal heterogeneity, driving factors, multi-source remote sensing data, carbon emission reduction strategies

*e-mail: zhujing@neuq.edu.cn
0000-0001-7451-3640

© 2026 This article is licensed under a Creative Commons Attribution-NonCommercial 4.0 International (CC BY-NC 4.0)

Introduction

Since the 1990s, rapid global industrialization and urbanization have resulted in a substantial increase in greenhouse gas emissions, giving rise to a series of environmental challenges, among which global climate change has attracted extensive international concern. During the same period, China's extensive production and energy-intensive development model have led to a sharp surge in carbon dioxide emissions, exerting considerable pressure on the ecological environment. Liaoning Province is a traditional industrial base in China, characterized by an industrial structure dominated by heavy industries. It is also one of the country's pilot provinces for carbon peaking, playing an important role in exploring sustainable pathways toward low-carbon transformation. Therefore, this study selects Liaoning Province as the research area to examine the spatiotemporal distribution characteristics of carbon dioxide emissions and their driving factors, intending to provide scientific support for developing rational and effective carbon emission reduction strategies that contribute to achieving China's goals of carbon peaking and carbon neutrality.

Existing research on the spatiotemporal evolution of carbon emissions suggests that nighttime light data provides a highly accurate basis for spatial modeling of carbon dioxide emissions. For example, studies integrating nighttime light data with statistical carbon emission inventories have adopted exploratory spatiotemporal data analysis frameworks to investigate the spatiotemporal patterns of China's carbon footprint [1]. Similarly, previous research has identified a strong correlation between DMSP-OLS nighttime light data and carbon emissions, allowing for the spatial allocation of energy-related carbon emissions based on this relationship [2]. Another study estimated carbon dioxide emissions for 2,735 counties in China using both DMSP-OLS and NPP-VIIRS nighttime light data, achieving robust model fitting performance following validation [3]. Nevertheless, the exclusive use of nighttime light data for spatial allocation remains insufficient for accurately capturing the spatial distribution of carbon emissions. It is therefore necessary to incorporate key driving factors that reflect the spatiotemporal heterogeneity of emissions. Identifying these drivers forms the theoretical foundation for designing effective carbon emission reduction policies. Numerous studies have examined the effects of energy structure, energy intensity, GDP, and population size on energy-related carbon emissions, with GDP consistently emerging as the most influential factor [4]. Other studies employing the STIRPAT model have analyzed the impacts of per capita GDP, total population, fossil fuel consumption, and GDP from commodity trade, revealing that GDP from commodity trade exerts the strongest influence on carbon emissions [5]. In addition, the LMDI model has been applied to investigate provincial-level determinants of carbon emissions, concluding that production efficiency serves as the primary factor constraining emission growth [6]. However, the multi-scale heterogeneity of these influencing factors remains insufficiently explored, indicating the need for further empirical investigation.

Therefore, this study centers on the spatiotemporal characteristics and driving factors of carbon dioxide emissions in Liaoning Province. Specifically, it simulates high-resolution spatial carbon emissions to examine their spatiotemporal evolution and to identify the key factors influencing these variations, with particular attention to the spatial heterogeneity of the driving mechanisms. The findings aim to provide a valuable reference for carbon emission reduction strategies in regions with similar socioeconomic and industrial structures.

The potential innovative points of this study are as follows: (1) Innovations in the research perspective. Taking into account the limitations of nighttime light data, this study integrates nighttime light data, population data, and land use data to downscale the provincial carbon emission data from the CEADs database to a 1 km × 1 km grid across three regions, thus achieving the spatial allocation of carbon emission data. By using the Mosaic to New Grid tool, we generated grid-scale carbon emission data for Liaoning Province, which not only improves the spatial accuracy of carbon emission data but also provides an innovative perspective for exploring the relationship between the temporal and spatial characteristics of carbon emissions and land types. (2) Innovations in the application of research methodology to the study area. Among the numerous studies that select Liaoning Province as the study area, few have investigated the temporal and spatial characteristics of carbon emissions and their influencing factors. This study examines the temporal and spatial characteristics of grid-scale carbon emissions in Liaoning Province and, innovatively, considers the impacts of the spatial location and spatial relationships among influencing factors on carbon emissions in the region. We adopted the Multi-Scale Geographically Weighted Regression (MGWR) model to examine the relationship between carbon emissions and their determinants in Liaoning Province. By integrating spatial statistics with regression methods, this study conducts modeling on explanatory variables under different spatial bandwidths, which better explains the spatial characteristics of carbon emissions in Liaoning Province and reduces the deviation between regression results and actual results (Fig. 1).

Study Area and Data

Study Area

This study selects Liaoning Province, China, as the research area. Situated in the southern part of Northeast China, the province extends from 38°43′N to 43°26′N and from 118°53′E to 125°46′E, covering an area of approximately 148,000 km^2, which represents about

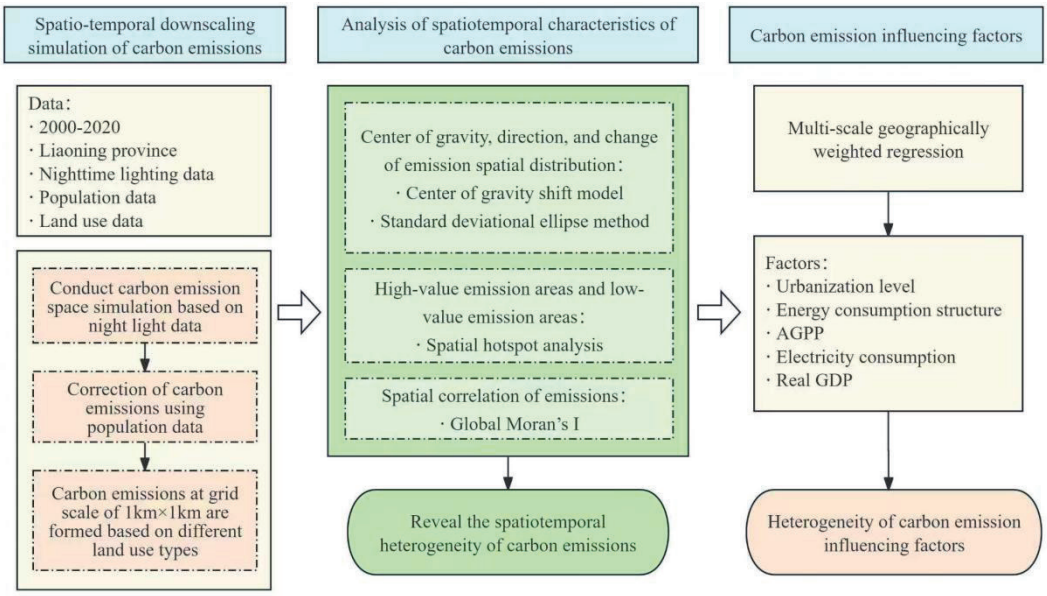

Fig. 1. Research framework.

1.5% of China's total land area. Liaoning consists of 14 prefecture-level cities. The province is rich in mineral resources, including iron ore and petroleum, which have laid the foundation for its heavy industry-dominated industrial structure and established it as one of China's traditional industrial bases. According to provincial carbon emission data released by Carbon Emission Accounts and Datasets (CEADs), Liaoning Province emitted 545.674 Mt of carbon dioxide in 2021, accounting for 5.27% of the national total.

Data Sources and Preprocessing

Physical Geography Data

The natural geographic data used in this study include land use data, Annual Gross Primary Productivity (AGPP) of Terrestrial Ecosystems, and Digital Elevation Model (DEM) data. The land use data were obtained from the Resource and Environment Science and Data Center of the Chinese Academy of Sciences, with a spatial resolution of 1 km × 1 km. Based on the relationship between different land use types and carbon dioxide emissions, ArcGIS was employed for data reclassification and preprocessing. Urban land and urban residential land were classified as Type 1, representing carbon emissions from urban residential consumption, construction, wholesale and retail trade, accommodation and food services, as well as transportation and postal sectors. Industrial land was classified as Type 2, representing industrial carbon dioxide emissions. Rural settlements, cropland, forest land, grassland, water bodies, and unused land were categorized as Type 3, representing rural residential emissions and those arising from agriculture, forestry, animal husbandry, fisheries, and water conservancy activities. This three-type land use classification system reflects the differentiated impacts of various land types on carbon dioxide emissions. The Annual Gross Primary Productivity (AGPP) of Terrestrial Ecosystems was obtained from China's Terrestrial Ecosystem AGPP dataset, and AGPP data for the study area were extracted and standardized. Digital Elevation Model (DEM) data were sourced from the Geographic Data Cloud and processed through mosaicking, cropping, and other standard processing procedures. Nighttime light data were acquired from the Harvard Dataverse platform, with a spatial resolution of 500 m × 500 m. These data were processed to exclude global water bodies, then projected, rasterized, and resampled. Finally, nighttime light data corresponding to urban and industrial areas were extracted and converted from raster to point format.

Socioeconomic Data

The population spatial distribution data were extracted and resampled. Carbon dioxide emissions data were obtained from CEADs. Emissions were calculated according to different land use types after reclassification. Actual GDP grid data and electricity consumption grid data had a spatial resolution of 1 km × 1 km. These datasets were subjected to raster projection, zonal statistics, and normalization processing. Energy consumption data were derived from the Liaoning Provincial Statistical Yearbook, while data on the urbanization rate were obtained from the China Statistical Yearbook. Both energy consumption and urbanization rate were rasterized using a density-based zoning method (Table 1).

Table 1. Data source.

Data Type	Data Name	Data Source
Physical Geography Data	Land Use Data	http://www.resdc.cn
	Annual Gross Primary Productivity of Terrestrial Ecosystems (AGPP)	http://www.csdata.org/
	DEM	gscloud.cn
Socioeconomic Data	Population Data	https://landscan.ornl.gov/
	Carbon Dioxide Emissions	Carbon Emission Accounts and Datasets (CEADs)
	Energy Consumption	Liaoning Statistical Yearbook
	Urbanization Rate	China Statistical Yearbook

Materials and Methods

Grid-Scale Carbon Dioxide Emissions Simulation

Among carbon dioxide emission accounting results at the Chinese administrative scale, the CEADs database stands out for its comprehensive coverage of emission sources and accounting scope, emission factors consistent with China's actual emission characteristics, continuous accounting time series, and widespread recognition [7-9]. This study adopts the CEADs database (2000-2020) carbon emission statistics as the overall carbon emissions for Liaoning Province. Based on these administrative-scale emissions, spatiotemporal downscaling simulations are conducted at the grid scale according to land use types, yielding a high-resolution 1 km × 1 km carbon emission profile.

NPP-VIIRS nighttime light data, population data, and land use data were used to perform spatiotemporal downscaling simulations of carbon emissions. First, spatial distribution simulations were conducted based on the relationship between energy consumption and carbon dioxide emissions represented by nighttime light data [10]. Second, because nighttime light data are insufficient to represent carbon dioxide emissions from rural settlements, cropland, forest land, grassland, water bodies, and unused land, population density data were employed to correct the simulated grid-scale emissions. Third, according to the relationship between land use types and carbon dioxide emissions, three categories were defined: urban land and urban residential land were classified as Category 1, industrial land as Category 2, and rural settlements, cropland, forest land, grassland, water bodies, and unused land as Category 3. Based on this classification, a 1 km × 1 km grid-scale spatial distribution pattern of carbon dioxide emissions in Liaoning Province was established. The specific formula is as follows [11].

$$C_r = \frac{DN_r}{DN_c} \times C_c \tag{1}$$

In Eq. (1), C_r represents the grid-scale carbon emissions, DN_r denotes the nighttime light index or population count for the grid scale, DN_C indicates the total nighttime light index or total population index within the region containing the grid data, and C_C signifies the total carbon dioxide emissions of that region.

Method for Analyzing the Spatiotemporal Characteristics of Carbon Emissions

Spatial Center, Direction, and Variation of Carbon Emissions

The center-of-mass shift model is employed to study the spatial distribution center, direction, and variation of carbon emissions, aiming to identify the spatial geometric location and its changes in the research object. Standard deviation ellipse analysis is used to investigate the directionality and variation of the research object in two-dimensional space. Parameters such as the azimuth and major/minor axes of the standard deviation ellipse characterize spatial fluctuation patterns tending toward equilibrium or polarization. The specific formulas are as follows:

$$\tan\theta = \left(\sum x_i'^2 - \sum y_i'^2\right) + \frac{\sqrt{\left(\sum x_i'^2 - \sum y_i'^2\right)^2 + 4\left(\sum x_i'^2 - \sum y_i'^2\right)^2}}{2\sum x_i'^2 - \sum y_i'^2} \tag{2}$$

$$\delta_x = \sqrt{\frac{\sum (x_i' \cos\theta - y_i' \sin\theta)^2}{n}} \tag{3}$$

$$\delta_y = \sqrt{\frac{\sum (x_i' \sin\theta - y_i' \cos\theta)^2}{n}} \tag{4}$$

In Eq. (2), Eq. (3), and Eq. (4), $\tan\theta$ represents the rotation angle, x_i' and y_i' denote the spatial displacement relative to the spatial mean along the X-axis and Y-axis, respectively, and δ_x and δ_y represent the deviations along the X-axis and Y-axis, respectively.

High-value and Low-value Areas of Carbon Emissions

Spatial hotspot analysis is applied to investigate the spatial distribution characteristics of high-emission zones and low-emission zones. Spatial hotspot analysis leverages the principle that geographically proximate objects or attributes are correlated and is typically used to measure the spatial clustering intensity of high or low values in a study subject. The specific formula is as follows:

$$G(d) = \frac{\sum_{i=1}^{n}\sum_{j=1}^{n} w_{ij}(d)x_i x_j}{\sum_{i=1}^{n}\sum_{j=1}^{n} x_i x_j}, i \neq j \quad (5)$$

In Eq. (5), $G(d)$ is the hotspot statistic value, x_i and x_j are the statistic values of raster *i* and raster *j,* respectively, *d* is the spatial distance between the statistic values of raster *i* and raster *j*, and w_{ij} is the spatial distance weight matrix of $x_i x_j$.

Spatial Correlation of Emissions

The Global Moran's *I* index reflects the spatial clustering characteristics of carbon emissions. Moran's I value ranges between [-1, 1]. A value >0 indicates positive spatial correlation in the carbon emissions distribution. The closer the value is to 1, the more spatially clustered the emissions are. A value <0 indicates spatially dispersed emissions, with values closer to -1 signifying more pronounced dispersion. A value of 0 indicates no correlation, meaning emissions follow a random distribution pattern. The specific formula is as follows:

$$I=\frac{n\sum_{i=1}^{n}\sum_{j=1}^{n} W_{ij}(X_i-\bar{X})(X_j-\bar{X})}{\sum_{i=1}^{n}\sum_{j=1}^{n} W_{ij}\sum_{i=1}^{n}(X_i-\bar{X})^2} \quad (6)$$

In Eq. (6), X_i represents the observed value of the unit, and W_{ij} denotes the standardized spatial weight matrix. *I* ranges from -1 to 1, where $I>0$ indicates positive correlation, $I<0$ indicates negative correlation, and $I = 0$ indicates random spatial distribution.

Multi-Scale Geographically Weighted Regression

The research concept of the Multi-scale Geographically Weighted Regression (MGWR) model originates from Generalized Additive Models (GAM). By integrating spatial statistics and regression methods, its advantage lies in allowing each independent variable to be modeled using different spatial bandwidths, thereby better explaining the heterogeneous characteristics of the dependent variable. To investigate the multidimensional socioeconomic and ecological factors influencing spatial heterogeneity in carbon emissions, the multi-scale geographically weighted regression model was employed to analyze the impact of multidimensional explanatory variables on carbon emissions. The specific formula is as follows:

$$y_i = \sum_{j=0}^{m} \beta_{bwj}(\mu_i, \nu_i)x_{ij} + \varepsilon_i \quad (7)$$

In Eq. (7), β_{bwj} represents the regression coefficient for the *j*-th independent variable, (μ_i, ν_i) denotes the center coordinates of the *i*-th study sample, and ε_i signifies the model error term. This study applies a Multi-Scale Geographically Weighted Regression (MGWR) model in ArcGIS to examine the determinants of carbon dioxide emissions in Liaoning Province and to reveal their spatiotemporal heterogeneity. Traditional geographically weighted regression (GWR) models use a single spatial bandwidth. In contrast, the MGWR model allows each variable to adopt its own optimal spatial bandwidth, which better captures the spatially heterogeneous characteristics of carbon emissions. Spatial bandwidths were therefore determined according to the principle of feature adjacency. The bandwidth range was adjusted based on the spatial distribution density of carbon emission-related evaluation units. Areas with dense features were assigned smaller spatial ranges, whereas areas with sparse features were assigned larger ranges. This procedure enabled the identification of the optimal spatial bandwidth and the appropriate number of adjacent features for each influencing factor. Drawing upon existing research on carbon emission determinants [12-15], we extracted multidimensional socioeconomic and ecological factors. Variables used in spatial downscaling simulations were excluded to ensure independence in model selection. Following collinearity tests, five factors were retained – urbanization level, energy consumption structure, AGPP, electricity consumption, and real GDP.

Results

Spatiotemporal Characteristics of Carbon Emissions

Overall, Liaoning Province's carbon emissions exhibited an upward trend from 2000 to 2020. Emissions rose from 208.957 Mt in 2000 to 533.285 Mt in 2020, representing a 155% increase and a significant overall growth. This evolution can be divided into two distinct phases. From 2010 to 2020, the growth rate slowed, with emissions increasing by only approximately 79 Mt in 2020 compared to 2010. Peak carbon emissions exhibited an overall fluctuating downward trend from 2000 to 2020, while the average value maintained continuous growth. The standard deviation showed a fluctuating pattern of "decline-rise-decline".

The spatial distribution of carbon emissions exhibits significant heterogeneity. Analysis of five selected emission periods reveals: In 2000, overall emissions remained low, with higher concentrations in the central region and Dalian City. From 2000 to 2005, Liaoning

Province's emissions increased overall, notably with a significant expansion of high-emission zones in central areas. From 2005 to 2010, high-emission zones expanded further in the central and coastal regions. In 2009, the Liaoning Coastal Economic Belt Development Strategy was elevated to a national strategy, bringing new development opportunities to the coastal areas and contributing to an upward trend in carbon emissions during this period. From 2010 to 2015, high-emission zones in Liaoning remained concentrated in the central region and coastal economic belt, though total emissions declined. Between 2015 and 2020, industrial restructuring and the phasing out of outdated production capacity yielded positive results, leading to an overall downward trend in carbon emissions within the Liaozhong Urban Agglomeration. From 2000 to 2020, overall high-emission areas significantly expanded and became more widespread, with central and coastal regions maintaining relatively high carbon emissions (Fig. 2).

Spatial Distribution Center of Carbon Emissions

From 2000 to 2020, the center of carbon emissions in Liaoning Province consistently resided within Anshan City, located in the province's central region. Overall, two significant spatial shifts occurred. The first notable shift took place between 2000 and 2005, with the center moving 22.24 km southwest. This shift may have been driven by the Chinese government's 2003 policy document, "Several Opinions on Implementing the Revitalization Strategy for Old Industrial Bases in Northeast China and Other Regions". Anshan,

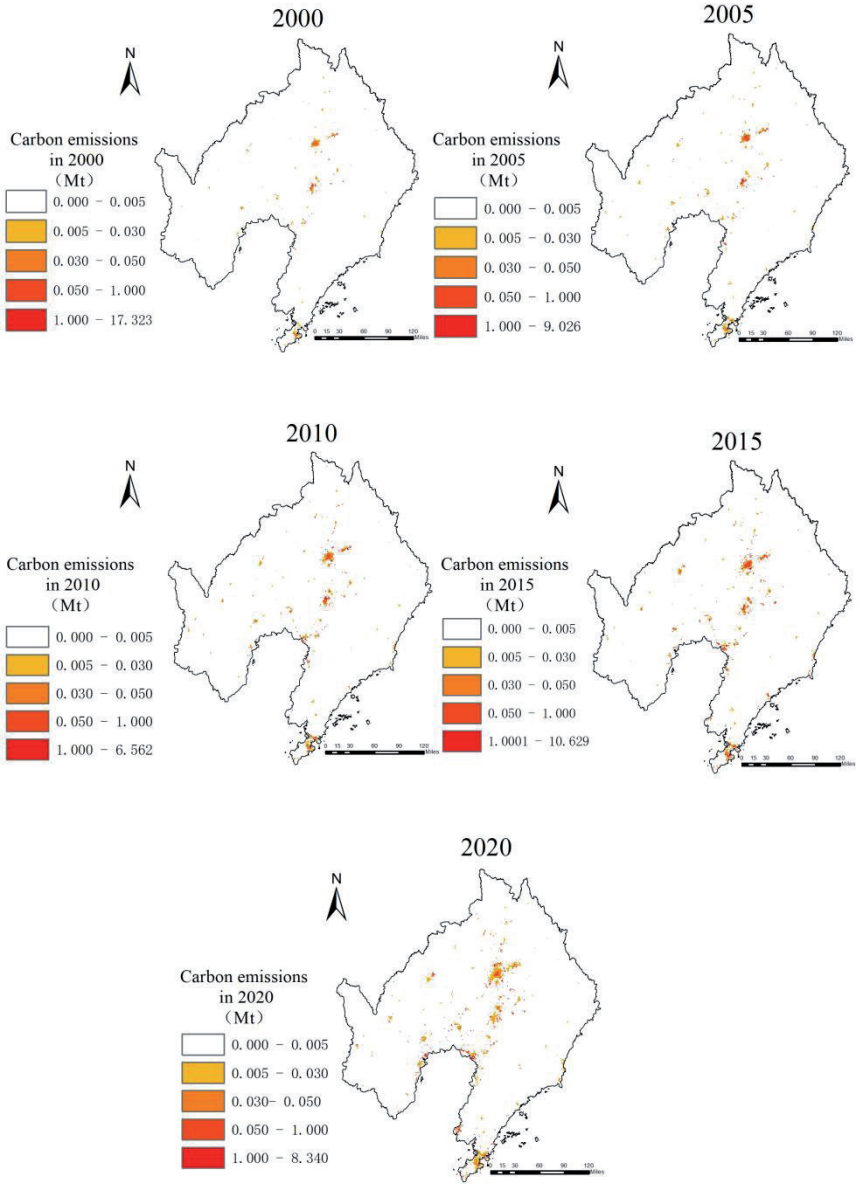

Fig. 2. Spatiotemporal distribution of carbon emissions (2000, 2005, 2010, 2015, 2020).

endowed with abundant mineral resources and holding the nation's largest iron ore reserves, featured a heavy industry-dominated industrial structure. During this period, Anshan experienced high growth rates in industrial added value for steel production, mineral product processing, light textiles, and equipment manufacturing, thereby establishing it as Liaoning's carbon emission center. A second significant spatial shift occurred between 2015 and 2020, moving 35.19 km southwest toward Panjin City and Yingkou City, marking a more pronounced shift than the first. A likely reason was the implementation of the Three-Year Plan for the Development of the Liaoning Coastal Economic Belt (2018-2020) in 2017. Liaoning Province prioritized the construction of the coastal economic belt, vigorously developing coastal economies and related marine industries. Additionally, between 2005 and 2015, Liaoning's carbon emission center remained relatively stable, consistently located in the central-southern region of the province. Overall, it exhibited a slight southwestward trend, gradually shifting toward the industrial base in central-southern Liaoning along the northern ring of Bohai Bay and the northwestern coast of the Yellow Sea (Fig. 3).

The standard deviation ellipse of carbon emissions is primarily centered on central Liaoning, exhibiting an overall northeast-southwest orientation. From 2000 to 2020, it gradually shifted from Tieling and Fushun in the northeast toward Panjin and Yingkou along the southwest coast. Within the standard deviation ellipse, the X-axis aligns in a "northwest-southeast" direction, while the Y-axis follows a "northeast-southwest" orientation. The north-south major axis is significantly longer than the east-west minor axis, indicating that carbon emissions in Liaoning Province are more concentrated along the north-south axis with lower dispersion. Conversely, east-west emissions exhibit uneven distribution, primarily concentrated in the central region. Specifically, from 2000 to 2005, both the X- and Y-axes of the standard deviation ellipse increased, indicating a gradual expansion in the concentrated distribution range of carbon emissions. From 2005 to 2010, the X-axis of the ellipse increased while the Y-axis shortened, suggesting a narrowing of the north-south distribution range during this period. From 2010 to 2015, both the X- and Y-axes of the standard deviation ellipse continued to increase, indicating an expansion in the spatial distribution of Liaoning Province's carbon emissions. Between 2015 and 2020, the standard deviation ellipse underwent significant changes: the X-axis increased markedly, with the westernmost point extending from Panjin City to Jinzhou City; the Y-axis shortened noticeably, shifting the northernmost point from Tieling City to Shenyang City (Fig. 4).

Spatial Aggregation Characteristics of Carbon Emissions

The spatial distribution of high-value (hotspot) and low-value (coldspot) carbon emission areas in Liaoning Province exhibits strong variability, with significant changes observed between 2000 and 2020. In 2000 and 2005, hotspots dominated the entire province, primarily concentrated in the central region. By 2010, the spatial

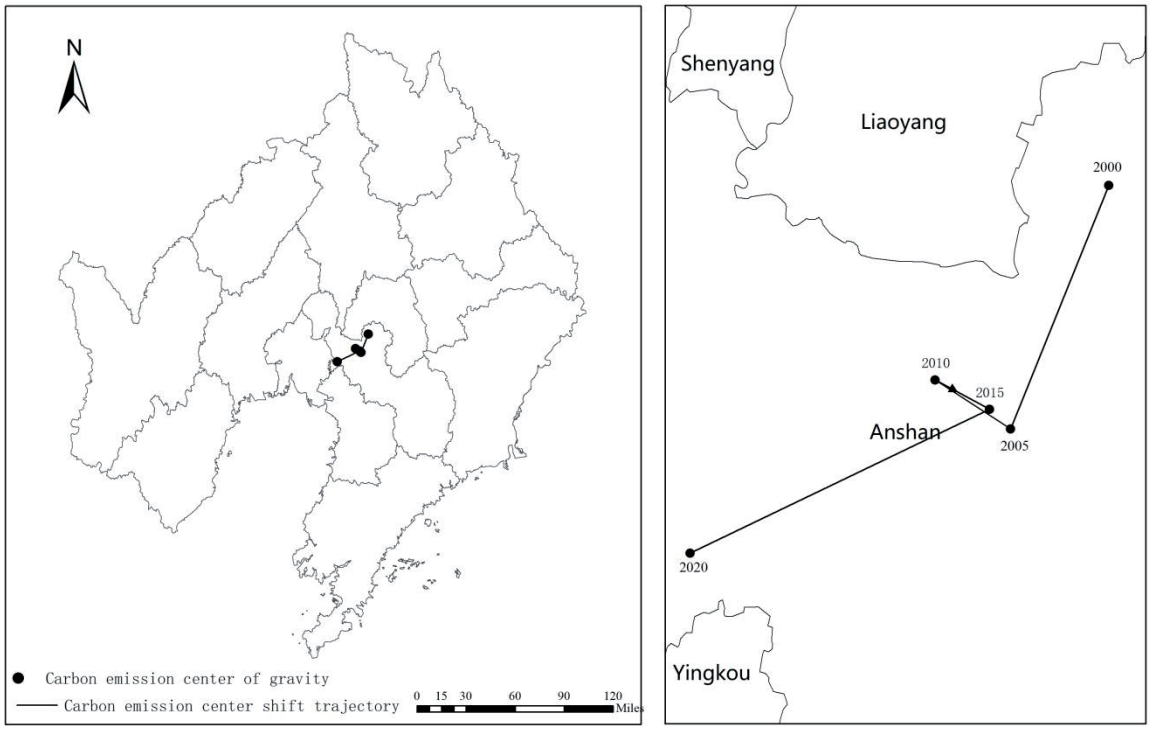

Fig. 3. Trajectory of carbon emission center shift (2000, 2005, 2010, 2015, 2020).

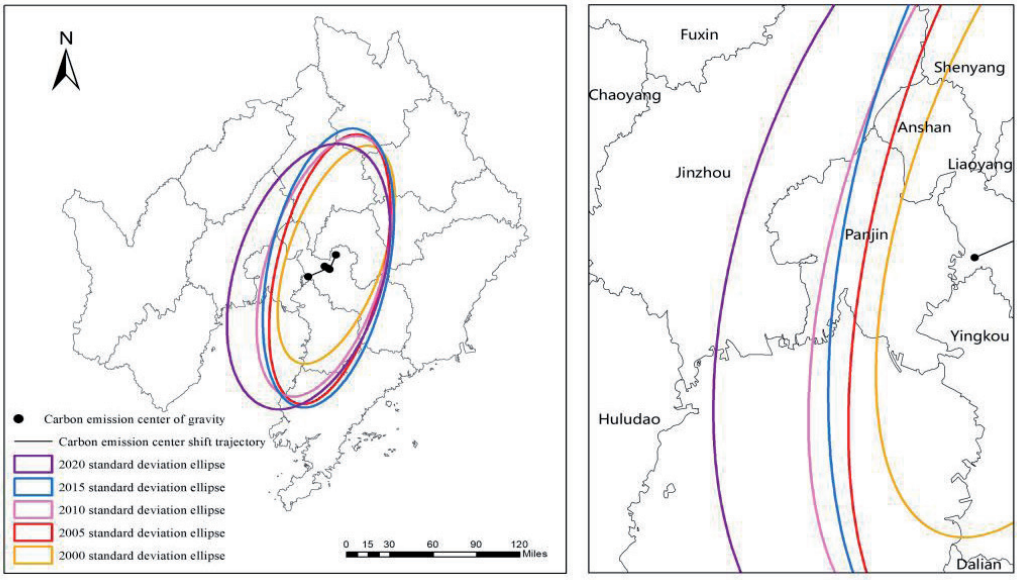

Fig. 4. Standard deviation ellipse of carbon emissions.

distribution pattern of carbon emission hotspots and coldspots underwent significant changes, with secondary coldspots becoming predominant. This shift closely aligns with China's energy conservation and emission reduction policies implemented during this period. Liaoning Province adopted measures such as phasing out outdated production capacity and promoting clean energy development, leading to a marked slowdown in carbon emission growth rates. By 2015, coldspots became predominant, with a small extreme hotspot concentrated near Shenyang in the central region. The pattern of carbon emission hotspots and coldspots remained largely stable by 2020, still dominated by coldspots. The southeastern region evolved into a secondary hotspot, while the northern Bohai Bay area emerged as an extreme hotspot (Fig. 5).

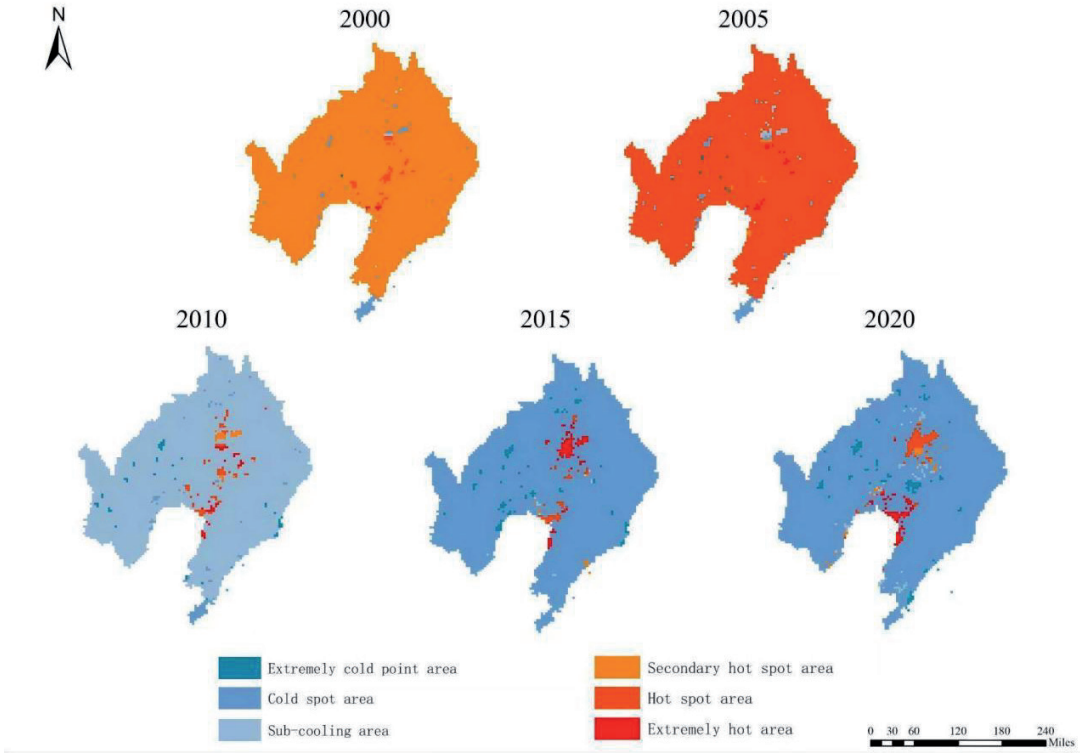

Fig. 5. Distribution of Carbon Emission Hotspots and Coldspots (2000, 2005, 2010, 2015, 2020).

Calculations of Moran's I index for carbon emissions revealed that the index exceeded 0 in all years (2000, 2005, 2010, 2015, 2020), with Z-values consistently above 0 and small P-values. The p-values for each study year were extremely low (0.000011 in 2000; 0.000000 in 2010, 2015, and 2020). These results lead to a strong rejection of the null hypothesis of random spatial distribution of carbon dioxide emissions at an exceptionally high confidence level. The findings indicate pronounced spatial clustering in carbon dioxide emissions across Liaoning Province throughout the study period. Areas with high emission levels and those with low emission levels both display clear spatial proximity. This indicates that the spatial distribution of carbon emissions is not random but exhibits positive spatial autocorrelation. Moran's I index values for carbon emissions from 2000 to 2020 showed minimal variation, indicating that carbon emissions in Liaoning Province remained relatively stable during the study period, with spatial clustering in a relatively stable state (Table 2).

Factors Influencing Carbon Emissions

The results indicate significant variations in the impact intensity of each factor on carbon emissions. The influence of various factors fluctuates across different time periods. On average, urbanization level shifted from a negative to a positive impact; energy consumption structure consistently exerted a positive promoting effect, with minimal variation across years except for a relatively minor impact in 2005; AGPP and

Table 2. Global Moran's I Index values for carbon emissions in Liaoning Province (2000, 2005, 2010, 2015, 2020).

	2000	2005	2010	2015	2020
Moran's I Index	0.071163	0.081911	0.112592	0.112378	0.076987
Expected Index	-0.006711	-0.004444	-0.003367	-0.002710	-0.001845
Variance	0.000313	0.000268	0.000204	0.000168	0.000073
z-score	4.404966	5.276876	8.125260	8.888049	9.246705
p-value	0.000011	0.000000	0.000000	0.000000	0.000000

Table 3. Factors influencing carbon emissions (2000, 2005, 2010, 2015, 2020).

Impact Factor	Regression Coefficient	Urbanization Level	Energy Consumption Structure	AGPP	Electricity Consumption	Real GDP
2000	Maximum	0.0633	20.9714	-0.0024	5.1945	0.3422
	Minimum	-0.0714	-1.3870	-0.0501	-0.8917	0.0669
	Mean	-0.0078	0.1409	-0.0156	-0.1010	0.2014
2005	Maximum	1.2273	0.0017	3.2833	0.4011	0.2256
	Minimum	-2.9617	-0.0013	-18.1534	-0.1567	0.0436
	Mean	-0.1048	0.0002	-0.0963	-0.0051	0.1402
2010	Maximum	8.3138	19.7821	0.0579	-0.0093	0.5421
	Minimum	-7.4445	-0.4926	-0.2820	-0.1144	0.2007
	Mean	-0.0747	0.1446	-0.0179	-0.0628	0.1419
2015	Maximum	0.1661	18.4494	0.0571	0.1299	-0.0285
	Minimum	-0.0795	-0.7824	-1.1571	-0.0493	-0.0355
	Mean	0.0123	0.1695	-0.0427	-0.0335	-0.0310
2020	Maximum	1.1262	2.3031	0.8085	0.0230	2.0929
	Minimum	-0.2685	-0.4308	-0.1525	0.0169	-0.9910
	Mean	0.0809	0.1429	0.0346	0.0198	0.0018

Note: The sign of regression coefficients in the model results indicates the direction of influence. The average value of regression coefficients indicates the overall direction of the primary correlations: a positive average value indicates a predominantly positive correlation, while a negative average value indicates a predominantly negative correlation. The magnitude of the average value represents the strength of the correlation - a larger average value indicates a stronger correlation.

electricity consumption both had positive effects in 2020 but maintained negative impacts in other years; actual GDP showed a negative impact in 2015 but positive effects in all other years (Table 3).

Discussion

This study focuses on the characteristics and influencing factors of carbon dioxide emissions at the provincial level in China. By employing spatial downscaling methods to simulate high-resolution carbon dioxide emission patterns, this study reveals their spatiotemporal heterogeneity and underlying determinants. The research aims to provide insights for identifying emission reduction pathways in China's typical carbon-emitting provinces.

Carbon Emissions Accounting

This study selected carbon emissions from the China Carbon Accounting Database as the foundational data for high-resolution emission simulations, based on factors such as the completeness of emission sources and the alignment of emission factors with China's localized characteristics. China's carbon accounting system has long relied on national macro-statistical data as its fundamental support. Macro-statistical data on energy consumption, industrial production, and related activities provide a reliable basis for obtaining activity-level information in carbon emission accounting [16, 17]. When combined with localized emission factors, these data more accurately reflect the actual characteristics of carbon emissions. Currently, carbon emission accounting is increasingly moving toward the integration of macro-statistical data with satellite remote sensing retrievals, enterprise-level online monitoring data, and other data sources, with the aim of further improving accounting accuracy [18, 19]. The carbon emissions accounted for in the China Carbon Accounting Database conform to China's macro-level statistical data system and reflect the fundamental characteristics of energy consumption and industrial production process emissions across China's 42 industrial sectors. It employs measured emission factors from various regions across China [20-23]. The CEADs database has established a comprehensive carbon accounting system characterized by detailed industrial sector disaggregation and measured emission factors, based on China's macro-statistical data and a bottom-up accounting framework. These emission data have gained widespread recognition and application in related research on China's carbon accounting [24]. In view of this, the present study also adopts the CEADs database as the fundamental data source. Compared with similar studies, this research provides a valuable reference for the high-resolution simulation of carbon emissions in typical high-emission regions.

The provincial sectoral emission data from CEADs were cross-validated against regional macroeconomic statistics, which not only ensured consistency in emission accounting at both the national and provincial levels but also enabled the tracking of interregional emission transfers across 42 industrial sectors [25-27]. In comparison with existing studies, for instance, it served as foundational data for urban carbon emissions in studies examining the spatiotemporal evolution of carbon emissions in resource-based cities of China's underdeveloped regions [28]. Other research utilized it as basic data to investigate influencing factors of carbon dioxide emissions at the prefecture-level city scale in China [29]. From the perspective of supporting regional emission reduction policy formulation, the CEADs database provides emission data at both provincial and sub-provincial administrative levels in China and has been widely applied in evaluating the effectiveness of local emission reduction policies. For example, in carbon emission studies of energy-abundant regions such as Ningxia, CEADs energy-related direct emission data have served as a core basis for quantifying emission reduction potential and informing policy design [30]. In addition, the long-term time-series dataset developed by CEADs through the integration of remote sensing imagery and multi-source statistical data offers a robust data foundation for analyzing the carbon lock-in effects of key emission-intensive industries, including oil refining and power generation, thereby supporting the identification of global emission hotspot transfer patterns and emission reduction priorities within the oil refining sector [31]. Additionally, some studies compared its emission quantities with those from the CEADs database to assess accounting consistency. Compared to using emission factor-based calculations as the data foundation for high-resolution emission simulations [32, 33], the carbon emissions selected in this study more accurately reflect the current emission status of the study area.

Spatiotemporal Downscaling Simulation of Carbon Emissions

Using emission factor-calculated carbon emission vector data as a foundation, multi-source data can be employed for spatiotemporal high-resolution downscaling simulations to obtain grid-scale carbon emission patterns, facilitating the revelation of spatial emission variations. Carbon emission accounting at the grid scale provides a critical foundation for accurately revealing the spatial distribution patterns and heterogeneity of carbon emissions. In general, substantial disparities exist in emissions among industrial clusters, agricultural production zones, and residential and service areas, which cannot be effectively distinguished using statistical data alone. Existing studies have shown that high-emission areas are typically concentrated in urban agglomerations and industrial clusters [34, 35], a finding that is consistent with the results of this study. Previous studies have predominantly relied on nighttime light data as the primary factor for downscaling

simulations. This is because areas with higher nighttime light values are generally considered to be more active in production and daily life, with relatively higher energy consumption leading to higher carbon emissions [32, 33, 36]. Therefore, this approach was also adopted in the present study, and the findings further corroborate this conclusion.

Building upon this foundation, this study further integrates population density, industrial structure characteristics, and land use type data to simulate carbon emissions at spatial scales. Multi-source data, including population density, industrial structure characteristics, and land use types, constitute the core foundation for refined spatial-scale simulation of carbon emissions. Population density captures the spatial agglomeration of emission demands such as energy consumption and transportation, with high-density population clusters typically corresponding to elevated carbon emissions from residential energy use [37]. From the perspective of industrial structure, regions dominated by secondary industries are generally characterized by high emission levels, whereas areas led by the service sector tend to exhibit relatively lower emission intensity [38]. In terms of land use types, industrial land and urban construction land consistently generate substantially higher carbon emissions than cultivated land and forest land [39, 40]. Compared with results derived from single-source statistical data, findings based on multi-source data demonstrate clear advantages in accuracy and spatial detail, thereby providing robust support for optimizing the spatial configuration of regional emission reduction strategies. Overall, spatial downscaling simulation of carbon emissions has become an essential tool for formulating refined and context-specific emission reduction policies. Compared to existing research, this study employs multi-source data from different dimensions and resolutions, including nighttime light data, land use types, and socioeconomic data, as the basis for high-resolution downscaling of carbon emissions. The conclusions regarding the spatial heterogeneity of carbon emissions based on land use types are consistent with previous studies [33].

Spatiotemporal Evolution Characteristics of Carbon Emissions

The study area features a heavy industry-dominated industrial structure, making it a typical high-energy consumption and high-emission region. Investigating the carbon emission characteristics of such areas provides valuable case studies for understanding emission patterns in similar regions. Regarding the temporal characteristics of carbon emissions, previous studies have classified emissions across 247 prefecture-level cities in China. Cities within this study area exhibit fluctuating growth and sustained growth patterns [29], consistent with the high-value emission fluctuations identified in this research. Since 2000, urban carbon emissions in China have exhibited clear phased evolutionary characteristics over time, including periods of rapid growth, decelerating growth rates, and increasing regional differentiation. Significant disparities in emission patterns exist between eastern coastal cities and emerging industrial cities in central and western China. Friedlingstein et al. pointed out that the gradient transformation pattern of urban carbon emissions in developing countries also supports this phenomenon [41]. Overall, China's urban carbon emissions have gradually shifted from nationwide synchronous growth toward regionally differentiated transformation [41, 42]. These conclusions regarding the temporal characteristics of China's urban carbon emissions are consistent with the findings of this study.

Regarding spatial evolution, prior studies have analyzed China's spatial carbon emission patterns since 2000. Findings indicate that central Liaoning Province and the coastal economic belt constitute high-emission zones exhibiting an overall downward trend [32]. Shenyang in central Liaoning and Dalian in the coastal economic belt are the primary carbon-emitting cities [33]. The distribution of carbon emission hotspots and coldspots aligns with the findings of this study [34], while simultaneously revealing a decoupling trend between carbon emissions and economic growth [7]. The spatial evolution of carbon emissions in Liaoning Province is closely associated with industrial transformation processes, variations in resource endowments, and regional development strategies. The high proportion of traditional energy-intensive industries, together with the spatial differentiation of resource endowments, has resulted in the persistent concentration of high-emission areas in cities such as Shenyang, Dalian, and Anshan since 2020. Among these cities, Shenyang has formed a localized carbon emission agglomeration primarily driven by traditional industries, including metal smelting and equipment manufacturing, whereas carbon emission clustering in Dalian is mainly attributable to port-related trade activities and petroleum processing industries. These findings are consistent with the conclusions of this study [43-48].

Factors Influencing Carbon Emissions

Existing research indicates that population, urbanization, GDP, industrial added value, energy consumption, and energy intensity are primary factors influencing carbon emissions. However, the magnitude of these factors' impact varies across China's provincial and prefecture-level cities [9, 29]. The spatial patterns and evolutionary characteristics of carbon emissions in Chinese cities are shaped by the interaction of multiple factors, among which industrial transformation, land use, and urban networks constitute the primary influencing dimensions. Empirical studies based on city-level data in China have demonstrated that the relationship between intensive land use and carbon emissions is constrained by the stage of urban development. Specifically, R&D investment intensity

exhibits a significant emission-reduction effect in middle-income cities; population density tends to suppress carbon emissions in both low- and middle-income cities, whereas capital investment intensity shows the most pronounced emission-promoting effect in low-income cities. These differentiated effects are closely associated with regional factor endowments and development stages. The results on influencing factors obtained in this study are consistent with the conclusions of existing research [49-52].

Some studies employ methods like geographic detectors to investigate influencing factors, facilitating pairwise comparisons of their relative impacts [32], while others use structural equation modeling to explore carbon emission. Some studies employ panel data at the Chinese city or regional level to conduct empirical analyses of the spatial heterogeneity of factors influencing carbon dioxide emissions [53-56]. Others focus on specific sectoral domains, such as the transportation sector, power sector, and manufacturing industry, further verifying the spatially heterogeneous characteristics of carbon dioxide emission drivers [57-59]. The findings consistently indicate that population size, economic development level, industrial structure, and energy consumption structure exert significant impacts on carbon dioxide emissions. However, due to differences in development stages, resource endowments, and geographic locations across regions and cities, both the direction and magnitude of these driving effects exhibit pronounced spatial variation. Given the pronounced spatial heterogeneity of the driving factors influencing urban carbon emissions, it is necessary to implement differentiated regional governance strategies. However, research on the heterogeneity of influencing factors remains insufficient. This study accounts for the spatial locations of both explanatory and response variables, modeling at different bandwidths to reduce regression errors and enhance the accuracy of results. It explains the varying degrees of influence of each factor on carbon emissions from a spatial heterogeneity perspective. The identification of spatiotemporal heterogeneity in influencing factors in this study enriches existing research and provides stronger empirical support for the formulation of differentiated, place-based emission reduction policies.

Conclusions

Liaoning Province, a typical high-energy-consumption and high-emission region in China, was selected as the study area. From 2000 to 2020, Liaoning's total carbon emissions exhibited a continuous upward trend, with growth rates gradually slowing since 2010. Spatial high-resolution simulations of Liaoning's carbon emissions reveal significant spatial heterogeneity. Overall, cities in the central region and coastal economic belt exhibit higher carbon emission levels, while eastern and western regions show lower values. From 2000 to 2020, the center of gravity of Liaoning's carbon emissions shifted from the northeast to the southwest, with the most pronounced migration occurring between 2015 and 2020. The standard deviation ellipse of Liaoning's carbon emissions primarily centers on the central region, exhibiting an overall "northeast-southwest" distribution pattern. It gradually shifts from the northeastern cities of Tieling and Fushun toward the southwestern coastal cities of Panjin and Yingkou. In 2000 and 2005, Liaoning's carbon emissions exhibited a spatial pattern dominated by hotspots, while coldspots became predominant in 2010. Overall, carbon emissions showed spatial autocorrelation and high-value clustering.

The urbanization level, energy consumption structure, AGPP, electricity consumption, and actual GDP are the primary factors influencing carbon emissions in Liaoning Province. The magnitude of their influence varies across regions. Taking 2020 as an example: Urbanization level exhibits a significant positive correlation; the positive correlation of energy consumption structure is spatially fragmented; AGPP shows a weak positive correlation with Liaoning's carbon emissions; electricity consumption correlates positively with Liaoning's carbon emissions, displaying a spatial pattern of lower correlation in the northwest and higher in the southeast; real GDP demonstrates a strong positive correlation with Liaoning's carbon emissions in the central region, though its correlation strength has decreased since the study's baseline year of 2000.

Policy Recommendations for Emission Reduction

First, urbanization levels from 2000 to 2020 showed a significant positive correlation with carbon emissions. During urbanization, it is essential to effectively prevent excessive energy consumption, increase the proportion of urban green spaces, and enhance urban carbon sinks. The urban scale should be scientifically and reasonably determined based on local carrying capacity, and the urban layout should be optimized. Second, energy consumption structure and carbon emissions showed a significant positive correlation from 2000 to 2020, predominantly in the central region. Therefore, developing clean energy, rationally optimizing energy consumption structures, improving energy efficiency, and promoting clean energy in the central region should be prioritized to curb carbon emissions. Third, from 2000 to 2020, AGPP (Agricultural, Forestry, and Grassland Products) primarily exhibited a negative impact on carbon emissions, concentrated in the central regions. In these areas, measures such as afforestation and reducing chemical fertilizer and pesticide use should be implemented to increase AGPP reserves, enhance carbon sequestration in forests and farmlands, and fully leverage AGPP's role in mitigating carbon emissions. Fourth, electricity consumption showed a positive correlation with carbon emissions from 2000

to 2020. Therefore, low-carbon retrofitting of coal-fired power plants should be implemented, reducing reliance on fossil fuels and upgrading the electricity sector. Fifth, industrial structure should prioritize developing high-tech industries, shifting away from extensive economic development patterns, reducing energy consumption, and continuously increasing the share of the tertiary sector.

Acknowledgments

This research was supported by Hebei Provincial Social Science Fund 2025 (No. HB25GL030).

Conflict of Interest

The authors declare no conflict of interest.

References

1. ZHANG Y.N., PAN J.H., ZHANG Y.J., XU J. Spatial-temporal characteristics and decoupling effects of China's carbon footprint based on multi-source data. Journal of Geographical Sciences, **31** (3), **2021**.
2. ELVIDGE C.D., BAUGH K.E., KIHN E.A., KROEHL H.W., DAVIS E.R., DAVIS C.W. Relation between satellite observed visible-near infrared emissions, population, economic activity and electric power consumption. International Journal of Remote Sensing, **18** (6), 1373, **1997**.
3. CHEN J., GAO M., CHENG S., HOU W., SONG M., LIU X., SHAN Y. County-level CO_2 emissions and sequestration in China during 1997-2017. Scientific Data, **7** (1), 391, **2020**.
4. XU S.C., HE Z.X., LONG R.Y. Factors that influence carbon emissions due to energy consumption in China: Decomposition analysis using LMDI. Applied Energy, **127**, 182, **2014**.
5. PAN B.B., ZHANG Y. Impact of affluence, nuclear and alternative energy on US carbon emissions from 1960 to 2014. Energy Strategy Reviews, **32**, 100581, **2020**.
6. XIAO P.N., ZHANG Y., QIAN P., LU M., YU Z., XU J., QIAN H. Spatiotemporal characteristics, decoupling effect and driving factors of carbon emission from cultivated land utilization in Hubei Province. International Journal of Environmental Research and Public Health, **19** (15), 9326, **2022**.
7. DU X., SHEN L., WONG S.W., MENG C., YANG Z. Night-time light data based decoupling relationship analysis between economic growth and carbon emission in 289 Chinese cities. Sustainable Cities and Society, **73**, 103119, **2021**.
8. HUO D., LIU K., LIU J.W., HUANG Y., SUN T., SUN Y., LIU Z. Near-real-time daily estimates of fossil fuel CO_2 emissions from major high-emission cities in China. Scientific Data, **9** (1), 684, **2022**.
9. ZHANG H.N., ZHANG X.P., YUAN J.H. Driving forces of carbon emissions in China: a provincial analysis. Environmental Science and Pollution Research, **28** (17), 21455, **2021**.
10. GHOSH T., ELVIDGE C.D., SUTTON P.C., BAUGH K.E., ZISKIN D., TUTTLE B.T. Creating a global grid of distributed fossil fuel CO_2 emissions from nighttime satellite imagery. Energies, **3** (12), 1895, **2010**.
11. LYU Z.G., GENG Y.S., LI W., YUE R. Integrating spatial carbon factors into ecological network construction in an energy-intensive megaregion toward multi-objective synergy in northern China. Environmental Impact Assessment Review, **106**, 107480, **2024**.
12. TANG D.C., ZHANG Y., BETHEL B.J. An analysis of disparities and driving factors of carbon emissions in the Yangtze River Economic Belt. Sustainability, **11** (8), 2362, **2019**.
13. CHEN W.D., YANG R.Y. Evolving temporal-spatial trends, spatial association, and influencing factors of carbon emissions in Mainland China: Empirical Analysis Based on Provincial Panel Data from 2006 to 2015. Sustainability, **10** (8), 2809, **2018**.
14. SONG J.K., SONG Q., ZHANG D., LU Y., LUAN L. Study on influencing factors of carbon emissions from energy consumption of Shandong Province of China from 1995 to 2012. Scientific World Journal, **2014** (1), **2014**.
15. LIU Y.L., CHANG X.L., HUANG C.F. Research and analysis on the influencing factors of China's carbon emissions based on a panel quantile model. Sustainability, **14** (13), 7791, **2022**.
16. DI VAIO A., CHHABRA M., ZAFFAR A., BALSALOBRE-LORENTE D. Accounting and Accountability in the Transition to Zero-Carbon Energy for Climate Change: A Systematic Literature Review. Business Strategy and the Environment, **34** (5), 5925, **2025**.
17. XU R., TONG D., XIAO Q., QIN X., CHEN C., YAN L., CHENG J., CUI C., HU H., LIU W., YAN X., WANG H., LIU X., GENG G., LEI Y., GUAN D., HE K., ZHANG Q. MEIC-Global-CO_2: A new global CO_2 emission inventory with highly-resolved source category and sub-country information. Science China-Earth Sciences, **66**, **2023**.
18. ZHENG B., TONG D., LI M., LIU F., HONG C., GENG G., LI H., LI X., PENG L., QI J., YAN L., ZHANG Y., ZHAO H., ZHENG Y., HE K., ZHANG Q. Trends in China's anthropogenic emissions since 2010 as the consequence of clean air actions. Atmospheric Chemistry and Physics, **18** (19), 14095, **2018**.
19. ALI R., REHMAN M.A., REHMAN R.U., NTIM C.G. Sustainable environment, energy and finance in China: evidence from dynamic modelling using carbon emissions and ecological footprints. Environmental Science and Pollution Research, **29** (52), 79095, **2022**.
20. SHAN Y., GUAN D., ZHENG H., OU J., LI Y., MENG J., ZHANG Q. China CO_2 emission accounts 1997-2015. Scientific Data, **5**, 170201, **2018**.
21. SHAN Y., HUANG Q., GUAN D., HUBACEK K. China CO_2 emission accounts 2016-2017. Scientific Data, **7** (1), 54, **2020**.
22. GUAN Y., SHAN Y., HUANG Q., CHEN H., WANG D., HUBACEK K. Assessment to China's recent emission pattern shifts. Earth's Future, **9** (11), e2021EF002241, **2021**.
23. XU J., GUAN Y., OLDFIELD J., GUAN D., SHAN Y. China carbon emission accounts 2020-2021. Applied Energy, **360**, 122837, **2024**.
24. QIN J., GONG N. The estimation of the carbon dioxide emission and driving factors in China based on machine learning methods. Sustainable Production and Consumption, **33**, 218, **2022**.

25. YU Y., SU J., DU Y. Impact of global value chain and technological innovation on China's industrial greenhouse gas emissions and trend prediction. International Journal of Environmental Science and Technology, **20** (12), 13347, **2023**.
26. LIU Z., GUAN D., WEI W., DAVIS S.J., CIAIS P., BAI J., HE K. Reduced carbon emission estimates from fossil fuel combustion and cement production in China. Nature, **524**, 335, **2015**.
27. ZHANG F., GALLAGHER K.S., DENG M.S., LIU H.R., ORVIS R., XUAN X.W. Assessing the Policy Gaps for Achieving China's Carbon Neutrality Target. Environmental Science and Technology, **59** (34), 18124, **2025**.
28. DONG H., ZHANG P., DONG H., JIA N. The spatiotemporal dynamic evolution characteristics of carbon emissions in less developed resource-based cities: evidence from Pingliang City, China. Scientific Reports, **15** (1), 11266, **2025**.
29. YANG X.L., JIN K., DUAN Z., GAO Y., SUN Y., GAO C. Spatial-temporal differentiation and influencing factors of carbon emission trajectory in Chinese cities - A case study of 247 prefecture-level cities. Science of the Total Environment, **928**, 172325, **2024**.
30. TANG Z., XIA X.S., HUANG Y.H., LU Y., GUO Z. Estimation of national forest aboveground biomass from multi-source remotely sensed dataset with machine learning algorithms in China. Remote Sensing, **14** (21), 5487, **2022**.
31. XIE J.C., QIN J.W., QIN X.Z., CUI D., LI Q., SUN D. Research on adaptive long-term time series carbon dioxide emission prediction model based on improved multilayer perceptron. Big Data Research, **42**, 100572, **2025**.
32. WEI W., ZHANG X., ZHOU L., XIE B., ZHOU J., LI C. How does spatiotemporal variations and impact factors in CO_2 emissions differ across cities in China? Investigation on grid scale and geographic detection method. Journal of Cleaner Production, **321**, 128933, **2021**.
33. ZHOU Y., CHEN M.X., TANG Z.P., ZHAO Y. City-level carbon emissions accounting and differentiation integrated nighttime light and city attributes. Resources, Conservation and Recycling, **182**, 106337, **2022**.
34. TAO, L., SU, Y., FANG, X. Global carbon emission spatial pattern in 2030 under INDCs: using a gridding approach based on population and urbanization. International Journal of Climate Change Strategies and Management, **14** (1), 78, **2022**.
35. CUI L., YANG H., MARTIN M., QIAO Y., ULRICH V., ZIPF A. Mapping High-Resolution Carbon Emission Spatial Distribution Combined with Carbon Satellite and Muti-Source Data. Remote Sensing, **17** (17), 3125, **2025**.
36. GUO B., XIE T.T., ZHANG W.C., WU H., ZHANG D., ZHU X., LUO P. Rasterizing CO_2 emissions and characterizing their trends via an enhanced population-light index at multiple scales in China during 2013-2019. Science of the Total Environment, **905**, 167309, **2023**.
37. QI W., LI G.D. Residential carbon emission embedded in China's inter-provincial population migration. Energy Policy, **136**, 111065, **2020**.
38. ZHANG X.S., HE S.C., MA L.D. Local environmental fiscal expenditures, industrial structure upgrading, and carbon emission intensity. Frontiers in Environmental Science, **12**, 1369056, **2024**.
39. LI L., HUANG X.J., YANG H. Optimizing land use patterns to improve the contribution of land use planning to carbon neutrality target. Land Use Policy, **135**, 106959, **2023**.
40. TAO J.B., KONG X.B. Spatial allocation of anthropogenic carbon dioxide emission statistics data fusing multi-source data based on Bayesian network. Scientific Reports, **11** (1), 18128, **2021**.
41. FRIEDLINGSTEIN P., O'SULLIVAN M., JONES M.W., ANDREW R.M., GREGOR L., HAUCK J., LE QUÉRÉ C., LUIJKX IT., OLSEN A., PETERS GP., PETERS W., PONGRATZ J., SCHWINGSHACKL C., SITCH S., CANADELL J.G., CIAIS P., JACKSON R.B., ALIN S.R., ALKAMA R., ARNETH A., ARORA V.K., BATES N.R., BECKER M., BELLOUIN N., BITTIG H.C., BOPP L., CHEVALLIER F., CHINI LP., CRONIN M., EVANS W., FALK S., FEELY R.A., GASSER T., GEHLEN M., GKRITZALIS T., GLOEGE L., GRASSI G., GRUBER N., GÜRSES Ö., HARRIS I., HEFNER M., HOUGHTON R.A., HURTT G.C., IIDA Y., ILYINA T., JAIN A.K., JERSILD A., KADONO K., KATO E., KENNEDY D., GOLDEWIJK K.K., KNAUER J., KORSBAKKEN JI., LANDSCHÜTZER P., LEFÈVRE N., LINDSAY K., LIU J.J., LIU Z., MARLAND G., MAYOT N., MCGRATH M.J., METZL N., MONACCI N.M., MUNRO D.R., NAKAOKA S.I., NIWA Y., O'BRIEN K., ONO T., PALMER P., PAN N.Q., PIERROT D., POCOCK K., POULTER B., RESPLANDY L., ROBERTSON E., RÖDENBECK C., RODRIGUEZ C., ROSAN T.M., SCHWINGER J., SÉFÉRIAN R., SHUTLER J.D., SKJELVAN I., STEINHOFF T., SUN Q., SUTTON A.J., SWEENEY C., TAKAO S., TANHUA T., TANS P.P., TIAN XJ., TIAN H.Q., TILBROOK B., TSUJINO H., TUBIELLO F., VAN DER WERF G.R., WALKER, A.P., WANNINKHOF R., WHITEHEAD C., WRANNE A.W., WRIGHT R., YUAN WP., YUE C., YUE X., ZAEHLE S., ZENG J.Y., ZHENG B. Global carbon budget 2022. Earth System Science Data, **14** (11), 4811, **2022**.
42. QIAN Y., WANG H., WU J.S. Spatiotemporal association of carbon dioxide emissions in China's urban agglomerations. Journal of Environmental Management, **323**, 116109, **2022**.
43. LIU B., LV J.H. Spatiotemporal Evolution and Tapio Decoupling Analysis of Energy-Related Carbon Emissions Using Nighttime Light Data: A Quantitative Case Study at the City Scale in Northeast China. Energies, **17** (19), 4795, **2024**.
44. LIU H., LIU Q., HE R., LI F., LU L. Decomposition analysis and decoupling effects of factors driving carbon emissions produced by electricity generation. Energy Reports, **11**, 2692, **2024**.
45. LYU J., LU S., LI X., LI Z., CAO C. Spatio-Temporal Characteristics of Industrial Carbon Emission Efficiency and Their Impacts from Digital Economy at Chinese Prefecture-Level Cities. Sustainability, **15** (18), 13694, **2023**.
46. XU S.J., CHENG H., ZHANG M.H., GUO K., LIU Q., GAO Y. Assessment and Adjustment of Export Embodied Carbon Emissions with Its Domestic Spillover Effects: Case Study of Liaoning Province, China. Sustainability, **14** (24), 16989, **2022**.
47. LI S.P., WANG Q., MENG Y. Analysis on the Status and Influencing Factors of Industrial Carbon Emissions in Northeast China. Advanced Materials Research, **869-870**, 866, **2013**.
48. QIAN X., YAN J., ZHANG S., ZHANG K. Exploring the Spatiotemporal Pattern Evolution of Carbon Storage in Northwestern China. Land Degradation & Development, **2025**.

49. ZHOU J., MA H., WANG S. Household consumption carbon emissions under different urbanization levels-A study based on micro-survey data. Cities, **158**, 105630, **2025**.
50. YANG S.J., WEN L.J., ZHANG A.L. The spatiotemporal response of land-use carbon emissions to climate change. Ecological Indicators, **170**, 112893, **2025**.
51. WANG H.P., LIU P.L. Characteristics of the urban environmental regulation network and its impact on carbon emission efficiency in China. Humanities & Social Sciences Communications, **11** (1), 1373, **2024**.
52. QI Y.W., PENG W.X. Effects of China's Regional Industrial Structure Adjustment on Carbon Emission Transfer Based on Gravity Model. Environmental Engineering and Management Journal, **18** (11), 2475, **2019**.
53. WANG N., QU Z.K., LI J., ZHANG Y., WANG H.Y., XI H., GU Z.L. Spatial-temporal patterns and influencing factors of carbon emissions in different regions of China. Environmental Research, **276**, 121447, **2025**.
54. GUO C., YU J. Determinants and their spatial heterogeneity of carbon emissions in resource-based cities, China. Scientific Reports, **14** (1), 5894, **2024**.
55. CHANG K.L., DU Z.F., CHEN G.J., ZHANG Y.X., SUI L.L. Panel estimation for the impact factors on carbon dioxide emissions: A new regional classification perspective in China. Journal of Cleaner Production, **279**, 123637, **2021**.
56. JIANG P., GONG X.J., YANG Y.R., TANG K., ZHAO Y.T., LIU S., LIU L. Research on spatial and temporal differences of carbon emissions and influencing factors in eight economic regions of China based on LMDI model. Scientific Reports, **13** (1), 7965, **2023**.
57. WANG X., FAN F.Y., LIU C.H., HAN Y.W., LIU Q.Y., WANG A.J. Regional differences and driving factors analysis of carbon emissions from power sector in China. Ecological Indicators, **142**, 109297, **2022**.
58. XU R., LIN B. Why are there large regional differences in CO_2 emissions? Evidence from China's manufacturing industry. Journal of Cleaner Production, **140**, 1330, **2017**.
59. LIU J., LI S., JI Q. Regional differences and driving factors analysis of carbon emission intensity from transport sector in China. Energy, **224**, 120178, **2021**.